

Performance Analysis of a Foreground Segmentation Neural Network Model

Joel Tomás Morais¹, António José Borba Ramires Fernandes¹, André Leite Ferreira² and Bruno Faria²

¹*Minho University*

²*Bosch Car Multimedia Portugal S.A.*

a70841@alunos.uminho.pt, arf@di.uminho.pt, {Andre.Ferreira2, Bruno.Faria}@pt.bosch.com

Keywords: Segmentation, Background Subtraction, FgSegNet_v2

Abstract: In recent years the interest in segmentation has been growing, being used in a wide range of applications such as fraud detection, anomaly detection in public health and intrusion detection. We present an ablation study of FgSegNet_v2, analysing its three stages: (i) Encoder, (ii) Feature Pooling Module and (iii) Decoder. The result of this study is a proposal of a variation of the aforementioned method that surpasses state of the art results. Three datasets are used for testing: CDNet2014, SBI2015 and CityScapes. In CDNet2014 we got an overall improvement compared to the state of the art, mainly in the LowFrameRate subset. The presented approach is promising as it produces comparable results with the state of the art (SBI2015 and Cityscapes datasets) in very different conditions, such as different lighting conditions

1 INTRODUCTION

Over the years object detection has seen different application domains with the aim of detecting an object type and location in a specific context of an image. Nevertheless, for some applications detecting an object location and type is not enough. For these cases, the labelling of each pixel according to its surroundings in an image presents itself as an alternative approach. This task is known as segmentation (Hafiz and Bhat, 2020) and finds applications in video monitoring, intelligent transportation, sports video analysis, industrial vision, amongst many other fields (Setitra and Larabi, 2014). Some of the techniques used in traditional segmentation include Thresholding, K-means clustering, Histogram-based image segmentation and Edge detection. Throughout the last years, modern segmentation techniques have been powered by deep learning technology.

Segmentation methods isolate the objects of interest of a scene by segmenting it into background and foreground. Throughout the aforementioned applications, segmentation is usually applied to localizing the objects of interest in a video using a fixed camera, presenting robust results.

Nevertheless, when the camera is not fixed or the background is changing, detecting objects of interest using background subtraction could be more demanding, generating diverse false positives. Moreover, it

demands a high computational cost when applied to videos (Liu et al., 2020). Another issue with the method consists in developing a self-adaptive background environment, accurately describing the background information. This can be challenging since the background could be changing a lot, e.g., in lighting and blurriness (Minaee et al., 2020).

After exploring numerous state of the art methods in this field, FgSegNet_v2 was chosen as a suitable candidate to explore since it outperforms every state of the art method in the (Wang, 2014) challenge. Through the analysis of its components, and exploring variations for each, we have achieved a more robust method that can cope with both fixed and moving cameras amongst datasets with different scenarios.

This work is organized as follows: section 2 describes the current state of the art in instance segmentation; section 3 presents FgSegNet_v2 architecture and our proposed variations; in section 4 we introduce the used metrics and datasets, followed by the experiments made in the FgSegNet_v2, followed by our results showing that the current implementation achieves state of the art performance. A conclusion and some avenues for future work are presented in section 5.

2 RELATED WORK

Background subtraction has been studied in the Statistics field since the 19th century (Chandola et al., 2009). Nowadays, this subject is being strongly developed in the Computer Science field, from using arbitrary to automated techniques (Lindgreen and Lindgreen, 2004), in Machine Learning, Statistics, Data Mining and Information Theory.

Some of the earlier background subtraction techniques are non-recursive, such as *Frame differencing*, *Median Filter* and *Linear predictive filter*, in which a sliding window approach is used for the background estimation (ching S. Cheung and Kamath, 2004), maintaining a buffer with past video frames and estimating a background model based on the statistical properties of these frames, resulting in a high consumption of memory (Parks and Fels, 2008). As for the recursive techniques, *Approximated Median Filter*, *Kalman filter* and *Gaussian related* do not keep a buffer for background subtraction, updating a single background based on the input frame (ching S. Cheung and Kamath, 2004). Due to the recursive usage, by maintaining a single background model which is being updated with each new video frame, less memory is going to be used when compared to the non-recursive methods (Parks and Fels, 2008).

Regarding segmentation, and using DL, the top state of the art techniques include Cascade CNN (Wang et al., 2017b), *FgSegNet_v2* (Lim and Keles, 2019) and *BSPVGAN* (Zheng et al., 2020). These methods have achieved the top three highest scores in the (Wang, 2014) challenge.

Cascade CNN (Wang et al., 2017b) is a semi-automatic method for segmenting foreground moving objects, it is an end-to-end model based on Convolutional Neural networks (CNN) with a cascaded architecture. This approach starts by manually selecting a sub-set of frames containing objects properly delimited, which are then used to train a model. The model embodies three networks, differentiating instances, estimating masks and categorizing objects. These networks form a cascaded structure, allowing them to share their convolutional features while also being able to generalize to cascades that have more stages, maintaining the prediction phase extremely fast.

In *FgSegNet_v2* (Lim and Keles, 2019), the aim is to segment moving objects from the background in a robust way under various challenging scenarios. It can extract multi-scale features within images, resulting in a sturdy feature pooling against camera motion, alleviating the need of multi-scale inputs to the network. A modified VGG 16 is used as an encoder

for the network, obtaining higher-resolution feature maps, which will be used as input for the Feature Pooling Module (FPM) and consequently as input for the decoder, working with two Global Average Pooling (GAP) modules.

BSPVGAN (Zheng et al., 2020) starts by using the median filtering algorithm in order to extract the background. Then, in order to classify the pixels into foreground and background, a background subtraction model is built by using Bayesian GANs. Last, parallel vision (Wang et al., 2017a) theory is used in order to improve the background subtraction results in complex scenes. Even though the overall results in this method don't outperform the *FgSegNet_v2*, it shows some improvements regarding lighting changes, outperforming other methods in Specificity and False Negative changes.

3 EXPLORING VARIATIONS FOR FGSEGNET_V2

In this section, an ablation study of the *FgSegNet_v2* components is presented, in order to potentially improve the previous method by reworking individually these components, obtaining a more robust method. The section is divided in different modules, starting from the details of the architecture, along with the description of the elements in it, i.e, Encoder, Feature Pooling module and Decoder, ending with the training details.

Following a segmentation strategy, the proposed work intends to segregate the background pixels from the foreground ones. In order to achieve this, a VGG-16 architecture is used as an encoder, in which the corresponding output is used as input to a FPM (Feature Pooling Module) and consequently to a decoder. The overall architecture can be seen in Figure 1.

3.1 Encoder

A modified version of VGG-16 (Simonyan and Zisserman, 2015) is used as the encoder, both in *FgSegNet_v2* and the proposed method, in which the dense layers and the last convolutional block were removed, leaving the current adaptation with 4 blocks. The first 3 blocks contain 2 convolutional layers, each block followed by a MaxPooling layer. The last block holds 3 convolutional layers, each layer followed by Dropout (Cicuttin et al., 2016). The architecture is depicted in Figure 2.

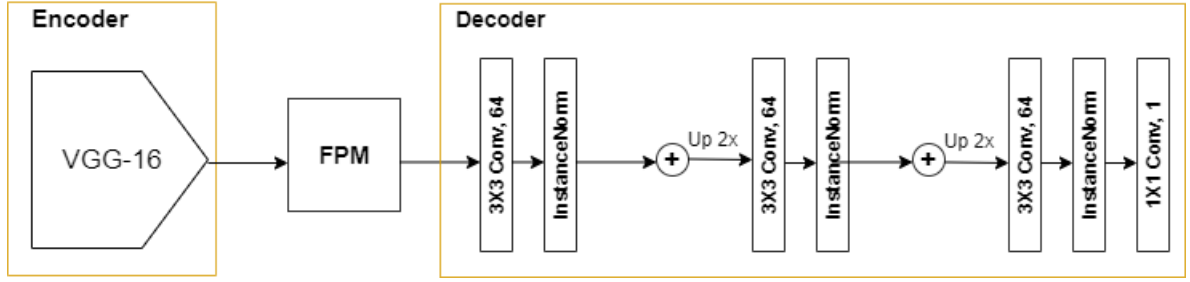


Figure 1: Proposed method architecture.

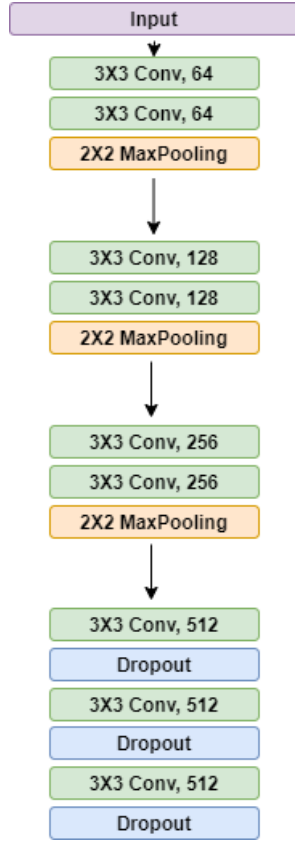


Figure 2: VGG-16 architecture.

After comparing this configuration with other models, i.e., Inception v_3, Xception and Inception ResNet v_2, we concluded that VGG-16 has given the best results so far, as seen in Section 4.4.3 . This allows the extraction of the input image features with high resolution, using these features as input to the FPM.

3.2 Feature Pooling Module

The Feature Pooling Module receives the features from the encoder in order to correlate them at differ-

ent scales, making it easier for the decoder to produce the corresponding mask.

Lim (Lim and Keles, 2019) proposed a Feature Pooling Module, in which the features from a 3 X 3 convolutional layer are concatenated with the Encoder features, resulting as input to the following convolutional layer with dilation rate of 4. The features from this layer are then concatenated with the Encoder features, hence used as input to a convolutional layer with dilation rate of 8. The process repeats itself to a convolutional layer with dilation rate of 8. The output of every layer is concatenated with a pooling layer, resulting in a 5 X 64 multi-features layers. These will finally be passed through InstanceNormalization and SpatialDropout.

After numerous experiments and tests, an improvement to this configuration was found. A convolutional layer with dilation rate of 2 is introduced, followed by the removal of the pooling layer. The output of the last layer, i.e., convolutional with dilation rate of 16, proceeds to BatchNormalization (Ioffe and Szegedy, 2015) (providing better results than InstanceNormalization) and SpatialDropout (Cicuttin et al., 2016) (Figure 3).

Due to the removal of the multi-features layers, SpatialDropout is used instead of Dropout. The former promoted independence between the resultant feature maps by dropping them in their entirety, correlating the adjacent pixels.

4 EXPERIMENTS AND RESULTS

When training is concluded, a test set containing the raw images and their corresponding masks is loaded, along with the trained model.

For each loaded image, a set of metrics are applied in order to evaluate the performance of the model. To complement these metrics, some visual results are also exploited. A probability mask is produced by applying a specific threshold in order to remove the low probability scores. These probabilities are translated

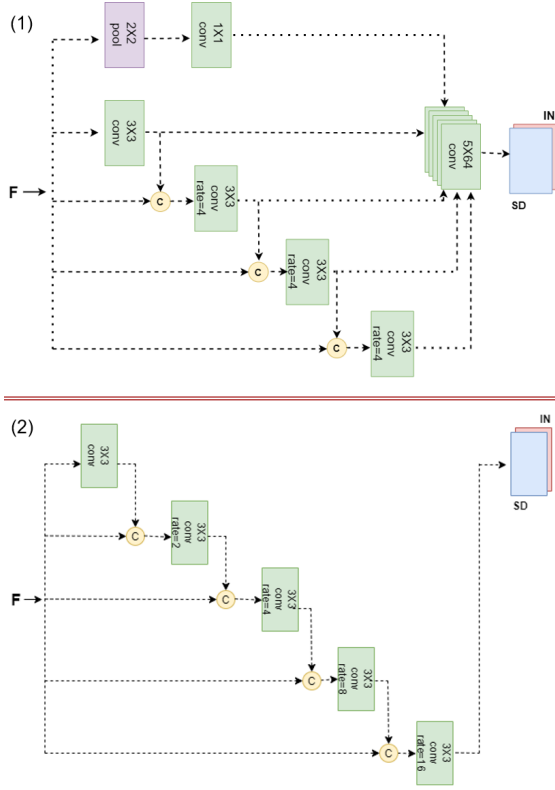


Figure 3: (1) Original Feature Pooling Module architecture and (2) Modified Feature Pooling Module architecture.

in a Jet heatmap, i.e., when the color is red there is a high probability of containing an object and when the color is purple there is a low probability, which will be blend with the corresponding raw image, making it easier to analyse the results.

4.1 Metrics

In order to fully understand the viability of the model, three different metrics are used throughout the evaluation. The first one is the *AUC* (Area Under Curve) (Flach et al., 2011), being equal to the probability that the classifier will rank a randomly chosen positive example higher than a randomly chosen negative example. This metrics allows the perception of the model detecting an object correctly, i.e., if the *AUC* is equal to 100% then the model detected every object in it. Nevertheless, this metric only focus on classification successes, failing to consider classification errors and not providing information regarding the segmentation. This metric plots two parameters: *TPR* (true positive rate) and *FPR* (false positive rate), seen in Equations 1 and 2.

$$TPR = \frac{TP}{TP+FN} \quad (1)$$

$$FPR = \frac{FP}{FP+TN} \quad (2)$$

The *Accuracy* and the *F-Measure* could be potential candidates, since they are highly used and usually produce reliable results, however, since the dataset is highly imbalanced when regarding the foreground and the background pixels, these two metrics are not an option, since they are highly sensitive to imbalanced data, therefore *MCC* (Mathews Correlation Coefficient) is used as an alternative (Chicco and Jurman, 2020), see Equation 3. This metric ranges from $[-1, +1]$ where $+1$ represents a perfect segmentation according to the ground truth, and -1 the opposite.

$$MCC = \frac{(TP \times TN) - (FP \times FN)}{\sqrt{(TP+FP)(TP+FN)(TN+FN)(TN+FP)}} \quad (3)$$

To complement the previous metric, *mIoU* (mean intersection over union) is also used. *IoU* is the area of overlap between the predicted segmentation and the ground truth divided by the area of union between the predicted segmentation and the ground truth, see Equation 4. When applied to a binary classification, a mean is computed by taking the *IoU* of each class and averaging them. This metric ranges from $[0, 1]$ where 1 represents a perfect overlap with the ground truth and 0 no overlap at all.

$$IoU = \frac{\text{Area of Overlap}}{\text{Area of Union}} \quad (4)$$

Metrics such as *Recall*, *Specificity*, *PWC* (*Percentage of wrong classifications*), *Precision* and *F-Measure* will also be used in some cases, in order to allow a comparison with other state of the art methods.

4.2 Datasets

Three different datasets are used to evaluate our proposal. The first one is *CityScapes*, which pretends to capture images regarding outdoor street scenes (Ramos et al.,). Every image was acquired with a camera in a moving vehicle across different months, this way different scenarios were covered, such as seasons and different cities. It has 20000 coarse pixel-level annotations, where 5000 of them were manually selected for dense pixel-level annotations. This way, there will be high diversity in foreground objects, background and scene layout. This dataset contains an additional challenge due to the moving camera.

The second is *CDNet2014* dataset (Wang et al., 2014), it consists of 31 camera-captured videos with

a fixed camera, containing eleven categories: Baseline, Dynamic Background, Camera Jitter, Intermittent Object Motion, Shadows, Thermal, Challenging Weather, Low Frame-Rate, Night, PTZ and Air Turbulence. The spatial resolution from the captured images ranges from 320x240 to 720x576. This dataset covers various challenging anomaly detections, both indoor and outdoor.

The last dataset is SBI2015 (Scene Background Initialization) (Christodoulidis and Anthimopoulos, 2015). It contains frames taken with a fixed camera from 14 video sequences with its corresponding ground-truths. It was assembled with the objective of evaluating and comparing the results of background initialization algorithms.

4.3 Training details

The proposed method receives a raw image and its corresponding mask, i.e., ground-truth, as input, both 512×512 . A pre-trained VGG-16 on ImageNet is used. The first three layer blocks of the VGG-16 are frozen in order to apply transfer learning to our model.

Binary cross entropy loss is used as the loss function, assigning more weight to the foreground in order to address the imbalance in the data, i.e., number of foreground pixels much higher than the background ones, and also taking in consideration when there are not any foreground pixels. The optimizer used is Adam (Kingma and Ba, 2015), as it provides better results amongst other tested optimizers, i.e., RMSProp, Gradient Descent, AdaGrad (Duchi et al., 2012) and AdaDelta (Zeiler, 2012), and the batch size is 4.

A maximum number of 80 epochs is defined, stopping the training if the validation loss does not improve after 10 epochs. The learning rate starts at $1e-4$, and is reduced after 5 epochs by a factor of 0.1 if the learning stagnates.

4.4 Experiments

Using (Lim and Keles, 2019) as a starting point, some ablation tests were made in CDNet2014 dataset using 25 frames for training, in order to understand the importance of the different components in the architecture and what could be improved. The metrics used throughout these evaluations are presented in 4.1.

Note that results presented in the following subsections have as only purpose the comparison of the proposed changes. Hence, these do not represent an improvement over the original FgSegNet.v2. Only when combined do these changes provide an increase in performance.

4.4.1 Feature Pooling Module

The goal is to break down the Feature Pooling Module, understanding its components and evaluate if improvements could be done.

The first stage consisted in changing the layers with different dilation rates, these dilated convolutions are used in order to systematically aggregate multi-scale contextual information without losing resolution (Yu and Koltun, 2016). The tests are (1) Removing the convolutional layer with dilation rate equal to 16, (2) Add a convolutional layer with dilation rate equal to 2 and (3) Add a convolutional layer with dilation rate equal to 2 and remove a convolutional layer with dilation rate equal to 16. As seen in Table 1, when removing the layer with dilation rate of 16, information is going to get lost, while when adding a layer with dilation rate equal to 2, better results are being obtained. Since adding a layer with dilation rate equal to 2 (2) improves the overall results, it will remain for the duration of the project.

The second stage is to change some of the concatenations between the layers. These tests consist in (1) Remove output from layer with dilation rate of 2 to the final concatenations, (2) Only concatenate layer with dilation rate=16 to the pooling and layer with $r=1$, (3) Delete every connection from pooling layer, (4) Only keep the final output of layer with dilation rate of 16 as input to the SpatialDropout and (5) Delete every concatenation.

As seen in Table 2, when comparing the concatenations, (4) produces the best results. Hence, the other concatenation tests will be discarded.

4.4.2 Decoder

The decoder in (Lim and Keles, 2019) uses three Convolutional layers 3×3 , followed by InstanceNormalization, and multiplies the output of the first two layers with the output of the Encoder and GlobalAveragePooling (GAP).

The first stage consists in analysing the importance of the GAP, maintaining the output of the Encoder or removing it (according to its corresponding GAP). The tests are (1) Remove the first GAP and its corresponding Encoder's output, (2) Remove the second GAP and its corresponding Encoder's output, (3) Remove both GAP and the Encoder's output, (4) Remove first GAP but keep the corresponding Encoder's output, (5) Remove second GAP but keep the corresponding Encoder's output and (6) Remove both GAP but keep both Encoder's output.

Table 1: Changing layers with different dilation rates in the Feature Pooling Module.

| | Baseline | | | LowFrameRate | | | BadWeather | | | CameraJitter | | |
|-----|---------------|---------------|---------------|---------------|---------------|---------------|---------------|---------------|---------------|---------------|---------------|---------------|
| | F-M. | MCC | mIoU | F-M. | MCC | mIoU | F-M. | MCC | mIoU | F-M. | MCC | mIoU |
| (1) | 0.9491 | 0.9313 | 0.9317 | 0.6250 | 0.6870 | 0.6930 | 0.8916 | 0.8817 | 0.8927 | 0.9030 | 0.8912 | 0.9000 |
| (2) | 0.9731 | 0.9697 | 0.9721 | 0.7102 | 0.7054 | 0.7098 | 0.9172 | 0.9102 | 0.9148 | 0.9218 | 0.9199 | 0.9205 |
| (3) | 0.9528 | 0.9487 | 0.9510 | 0.6970 | 0.6890 | 0.6900 | 0.9034 | 0.8987 | 0.9019 | 0.9190 | 0.9076 | 0.9119 |

Table 2: Changing concatenations between layers in the Feature Pooling Module.

| | Baseline | | | LowFrameRate | | | BadWeather | | | CameraJitter | | |
|-----|---------------|---------------|---------------|---------------|---------------|---------------|---------------|---------------|---------------|---------------|---------------|---------------|
| | F-M. | MCC | mIoU | F-M. | MCC | mIoU | F-M. | MCC | mIoU | F-M. | MCC | mIoU |
| (1) | 0.9281 | 0.9198 | 0.9260 | 0.6623 | 0.6596 | 0.6602 | 0.8916 | 0.8897 | 0.8904 | 0.9082 | 0.9047 | 0.9058 |
| (2) | 0.9528 | 0.9502 | 0.9516 | 0.6898 | 0.6885 | 0.6890 | 0.8994 | 0.8978 | 0.8983 | 0.9036 | 0.9011 | 0.9023 |
| (3) | 0.9804 | 0.9789 | 0.9799 | 0.7328 | 0.7311 | 0.7320 | 0.9207 | 0.9200 | 0.9202 | 0.9386 | 0.9368 | 0.9374 |
| (4) | 0.9824 | 0.9817 | 0.9820 | 0.7517 | 0.7502 | 0.7513 | 0.9305 | 0.9296 | 0.9300 | 0.9492 | 0.9486 | 0.9490 |
| (5) | 0.9528 | 0.9518 | 0.9520 | 0.6917 | 0.6909 | 0.6912 | 0.8923 | 0.8917 | 0.8920 | 0.9029 | 0.9010 | 0.9019 |

Table 3: Changes in the Decoder, by changing the configuration of the GAP.

| | Baseline | | LowFrameRate | |
|-----|---------------|---------------|---------------|---------------|
| | F-M. | MCC | F-M. | MCC |
| (1) | 0.9527 | 0.9502 | 0.8010 | 0.7927 |
| (2) | 0.9683 | 0.9650 | 0.8438 | 0.8412 |
| (3) | 0.9856 | 0.9851 | 0.9680 | 0.9655 |
| (4) | 0.8716 | 0.8678 | 0.7617 | 0.7600 |
| (5) | 0.9628 | 0.9611 | 0.8017 | 0.8000 |
| (6) | 0.8847 | 0.8826 | 0.7729 | 0.7711 |

Table 4: Changes in the Decoder, by changing the multiplications between the GAP and the dense layers.

| | Baseline | | LowFrameRate | |
|-----|----------|--------|--------------|--------|
| | F-M. | MCC | F-M. | MCC |
| (1) | 0.8926 | 0.8911 | 0.8618 | 0.8601 |
| (2) | 0.9327 | 0.9316 | 0.9137 | 0.9122 |
| (3) | 0.9126 | 0.9111 | 0.9017 | 0.8985 |

As seen in Table 3, (4) and (6) produce the worst results, decreasing the AUC, MCC and mIoU. As for the other configurations, they produce an overall increase in every metric. When removing both GAP modules and the Encoder’s outputs, option (3), the MCC and mIoU record the highest values, therefore the other configurations will be discarded.

After analysing the GAP, the relevance of the multiplications between the output of the first two layers in the Decoder and the output of the Encoder after applying the GAP must be considered. Therefore, additional tests were performed: (1) Remove first multiplication, (2) Remove second multiplication and (3) Remove both multiplications.

As seen in Table 4 the results decrease when compared to (3) from the previous stage (Table 3), hence these configurations will be discarded.

Table 5: Different Encoders.

| | Baseline | | LowFrameRate | |
|-----|----------|--------|--------------|--------|
| | F-M. | MCC | F-M. | MCC |
| (1) | 0.8816 | 0.8798 | 0.8126 | 0.8109 |
| (2) | 0.9014 | 0.9002 | 0.8428 | 0.8406 |
| (3) | 0.9218 | 0.9202 | 0.8828 | 0.8811 |

4.4.3 Encoder

Keeping the previous configurations of the FPM and the Decoder, three tests were made in the Encoder, changing the VGG-16 backbone to (1) Inception v3 (Szegedy et al., 2016), (2) Xception (Chollet, 2017) and (3) Inception ResNet v2 (Szegedy et al., 2017).

When comparing these three models with VGG-16, the latter produces better results in every metric, e.g., in the F-Measure and MCC as seen in Table 5, while also keeping the number of parameters much lower. Therefore no changes were made when compared to the FgSegNet.v2.

4.5 Final results and Comparison

With the previous configurations established, some results applied to the full datasets are compared with the state of the art.

Regarding the CDNet2014 dataset, the proposed method outperforms the top state of the art technique in this dataset, i.e., *FgSegNet.v2*, when using 200 frames for training, improving by a long margin the LowFrameRate class, going from 0.8897 to 0.9939 in the F-Measure, more details in Table 6. Some visual results can also be seen in Figure 4, presenting results close to the ground truth, even when dealing with LowFrameRate images.

In the SBI2015 dataset, the overall F-Measure decreased from 0.9853 to 0.9447 when compared with

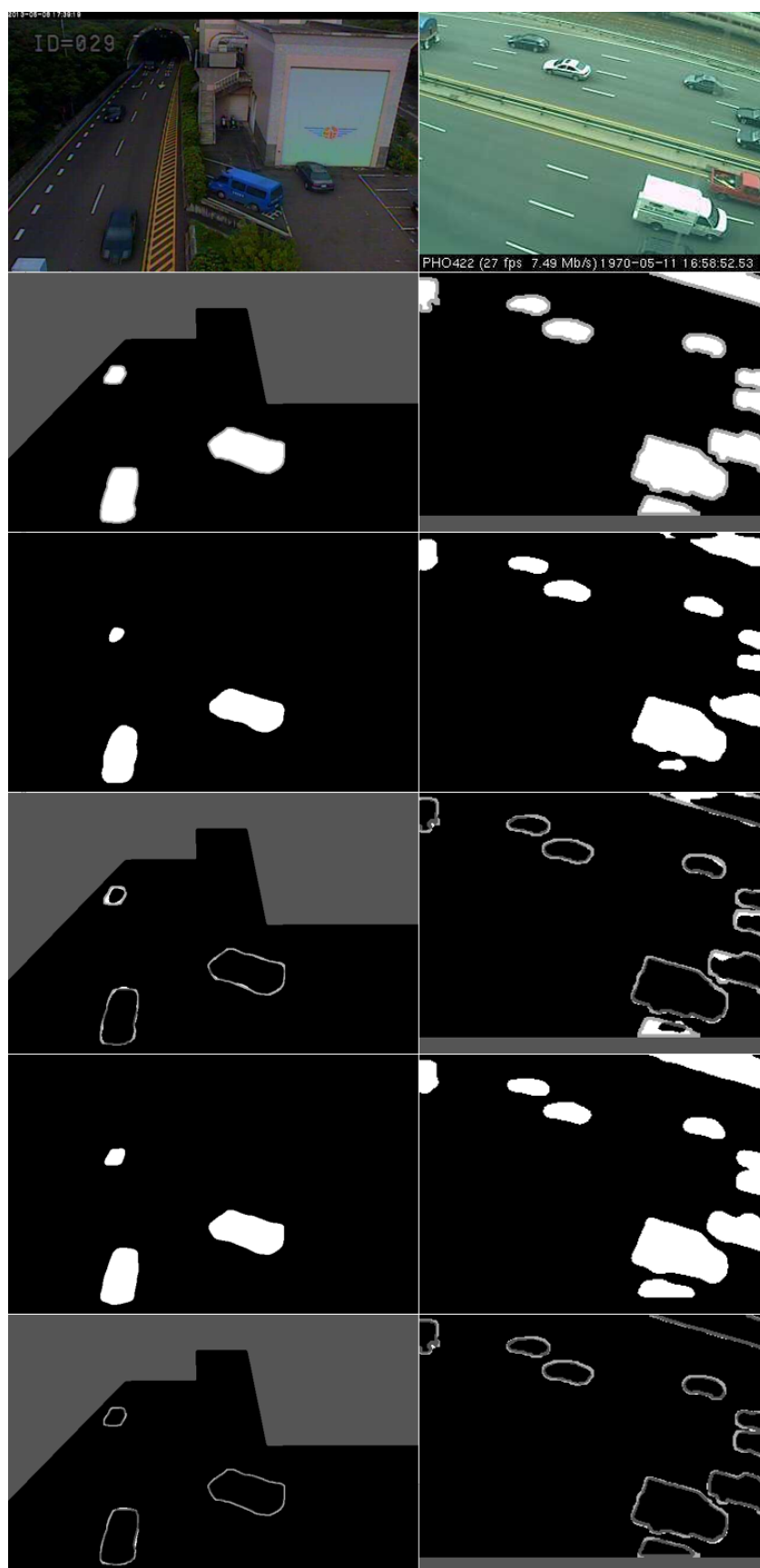


Figure 4: Results comparison in the LowFrameRate class. The rows represent raw images, ground-truth, FgSegNet_v2 output masks, difference between FgSegNet_v2 and ground truth, our proposed method output masks and difference between our proposed method and ground truth, respectively.

Table 6: Results comparison between (1) Our proposed method and (2) FgSegnet v2 using 200 frames for training across the 11 categories.

| | | FPR | FNR | Recall | Precision | PWC | F-Measure |
|---------------------|-----|---------------|---------------|---------------|------------------|---------------|------------------|
| Baseline | (1) | 6e-4 | 2e-3 | 0.9979 | 0.9974 | 0.0129 | 0.9975 |
| | (2) | 4e-5 | 3.8e-3 | 0.9962 | 0.9985 | 0.0117 | 0.9974 |
| Low Fr. | (1) | 4.8e-3 | 4.1e-3 | 0.9956 | 0.9910 | 0.0569 | 0.9939 |
| | (2) | 8e-5 | 9.5e-2 | 0.9044 | 0.8782 | 0.0299 | 0.8897 |
| Night V. | (1) | 7.4e-4 | 1.5e-2 | 0.9848 | 0.9785 | 0.1245 | 0.9816 |
| | (2) | 2.2e-4 | 3.6e-2 | 0.9637 | 0.9861 | 0.0802 | 0.9747 |
| PTZ | (1) | 6e-4 | 2.3e-2 | 0.9888 | 0.9902 | 0.0471 | 0.9922 |
| | (2) | 4e-5 | 2.1e-2 | 0.9785 | 0.9834 | 0.0128 | 0.9809 |
| Turbulence | (1) | 3e-4 | 2.5e-2 | 0.9861 | 0.9826 | 0.0417 | 0.9878 |
| | (2) | 1e-4 | 2.2e-2 | 0.9779 | 0.9747 | 0.0232 | 0.9762 |
| Bad Wea. | (1) | 1.3e-4 | 1e-2 | 0.9913 | 0.9914 | 0.0379 | 0.9881 |
| | (2) | 9e-5 | 2.1e-2 | 0.9785 | 0.9911 | 0.0295 | 0.9848 |
| Dyn.Back. | (1) | 3e-5 | 7.4e-3 | 0.9958 | 0.9959 | 0.0067 | 0.9960 |
| | (2) | 2e-5 | 7.5e-3 | 0.9925 | 0.9840 | 0.0054 | 0.9881 |
| Cam.Jitter | (1) | 1.6e-4 | 2.5e-3 | 0.9974 | 0.9940 | 0.0275 | 0.9957 |
| | (2) | 1.2e-4 | 9.3e-3 | 0.9907 | 0.9965 | 0.0438 | 0.9936 |
| Int.Obj.Mot. | (1) | 2.3e-4 | 7.4e-3 | 0.9925 | 0.9972 | 0.0672 | 0.9948 |
| | (2) | 1.5e-4 | 1e-2 | 0.9896 | 0.9976 | 0.0707 | 0.9935 |
| Shadow | (1) | 4e-4 | 1.6e-2 | 0.9909 | 0.9942 | 0.0542 | 0.9938 |
| | (2) | 1e-4 | 5.6e-3 | 0.9944 | 0.9974 | 0.0290 | 0.9959 |
| Thermal | (1) | 2e-4 | 2.7e-3 | 0.9972 | 0.9954 | 0.0302 | 0.9963 |
| | (2) | 2.4e-4 | 8.9e-3 | 0.9911 | 0.9947 | 0.0575 | 0.9929 |

Table 7: Results on the SBI dataset on 13 categories.

| | AUC | F-M. | MCC |
|-------------------------|------------|-------------|------------|
| Board | 99.84 | 0.9734 | 0.9724 |
| Candela | 99.92 | 0.9640 | 0.9631 |
| CAVIAR1 | 97.25 | 0.9475 | 0.9466 |
| CAVIAR2 | 97.51 | 0.9011 | 0.9001 |
| Cavignal | 99.94 | 0.9881 | 0.9872 |
| Foliage | 99.10 | 0.9124 | 0.9115 |
| HallAndMonitor | 98.49 | 0.9169 | 0.9160 |
| Highway1 | 99.35 | 0.9593 | 0.9583 |
| Highway2 | 99.56 | 0.9528 | 0.9518 |
| Humanbody2 | 99.82 | 0.9579 | 0.9580 |
| IBMtest2 | 99.42 | 0.9521 | 0.9512 |
| PeopleAndFoliage | 99.77 | 0.9570 | 0.9560 |
| Snellen | 98.84 | 0.8977 | 0.8967 |

Table 8: Results in the CityScapes dataset in the class Road, Citizens and Traffic Signs.

| | AUC | MCC | mIoU |
|----------------------|------------|------------|-------------|
| Road | 99.61 | 0.9555 | 0.9564 |
| Citizens | 99.31 | 0.7552 | 0.8019 |
| Traffic Signs | 97.72 | 0.6618 | 0.7425 |

tested in such dataset. A test was made in three different classes (Road, Citizens and Traffic Signs). As seen in Table 8 and in Figure 5, the proposed method is able to detect almost every object, confirmed by AUC metric.

the *FgSegNet_v2*, but increased from 0.8932 to 0.9447 when compared with the CascadeCNN, (Wang et al., 2017b). Nevertheless, the results still confirm a good overall evaluation on this dataset, compensating the higher results assembled in the CDNet2014 dataset. More details can be seen in Table 7.

Last, some preliminary tests (without direct comparison to other datasets) were made in the CityScapes dataset in order to evaluate the behaviour of the proposed method in a dataset with complex background changes, since *FgSegNet_v2* was not

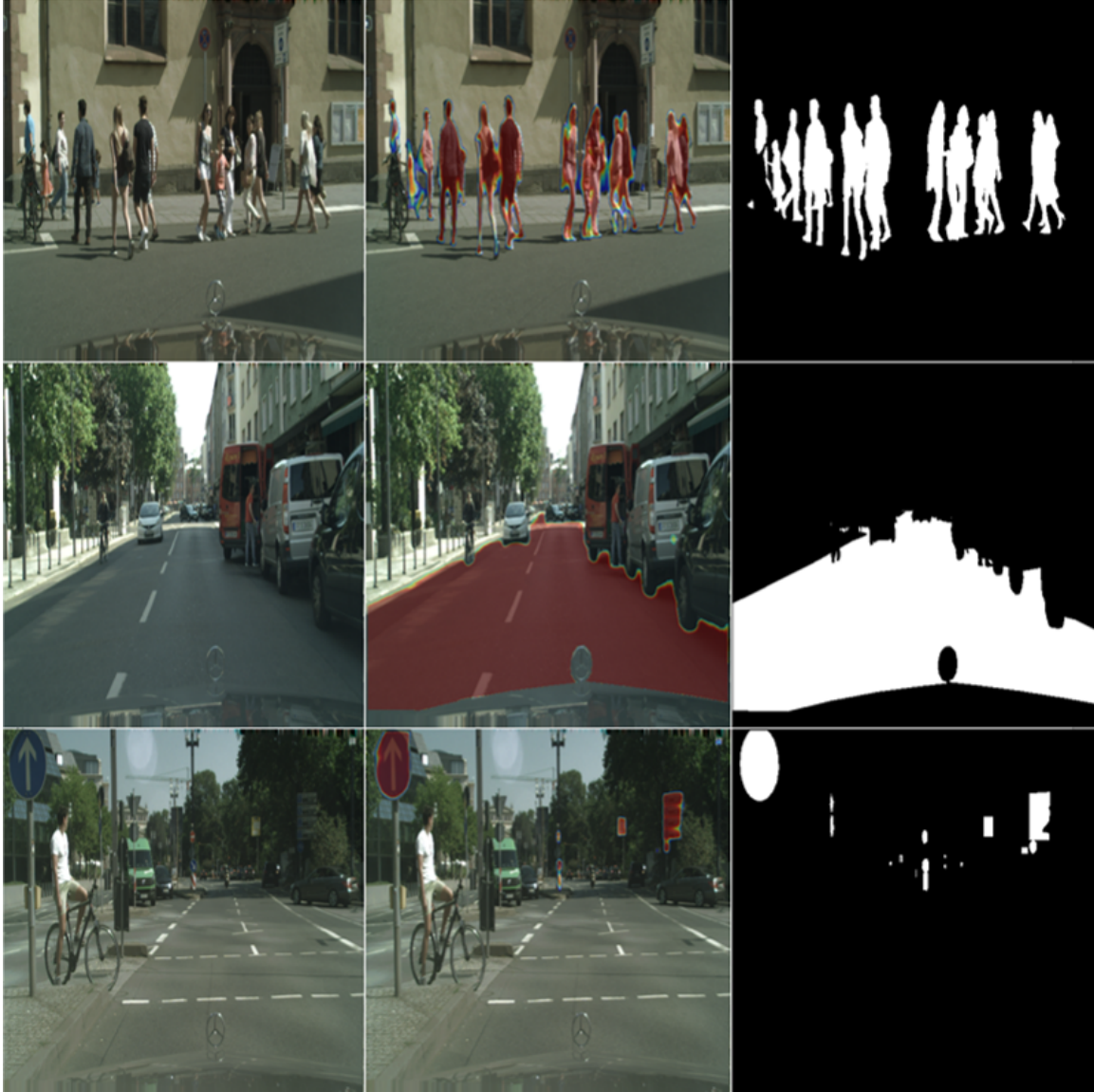


Figure 5: Results comparison in the CityScapes dataset. The columns represent raw images, our proposed method output mask and ground truth, respectively. The first row corresponds to Citizens class, second row to Road class and last two to Traffic Signs class.

5 CONCLUSION

An improved FgSegNet_v2 is proposed in the presented paper. By changing the Feature Pooling Module, i.e., deleting the pooling layer and only maintaining the output from the layer with dilation rate of 16, and the Decoder, i.e., removing the GAP modules, a more simplified and efficient approach is made, preserving the low number of needed training images feature while improving the overall results. It outperforms every state of the art method in the *ChangeDetection2014* challenge, in particular in the *LowFram-*

eRate images, showing a very significant improvement and also maintaining great results in the SBI and CityScapes datasets, resulting in a more generalized method than the others since no experiments have been shown when using these datasets simultaneously. As future work, we are going to focus on the *CityScapes* dataset, maintaining or improving the good results in other datasets.

ACKNOWLEDGEMENTS

This work is supported by: European Structural and Investment Funds in the FEDER component, through the Operational Competitiveness and Internationalization Programme (COMPETE 2020) [Project n° 039334; Funding Reference: POCI-01-0247-FEDER-039334].

This work has been supported by national funds through FCT – Fundação para a Ciência e Tecnologia within the Project Scope: UID/CEC/00319/2019.

REFERENCES

- Chandola, V., BANERJEE, A., and KUMAR, V. (2009). Survey of Anomaly Detection. *ACM Computing Survey (CSUR)*, 41(3):1–72.
- Chicco, D. and Jurman, G. (2020). The advantages of the Matthews correlation coefficient (MCC) over F1 score and accuracy in binary classification evaluation. *BMC Genomics*, 21(1):1–13.
- ching S. Cheung, S. and Kamath, C. (2004). Robust techniques for background subtraction in urban traffic video. In Panchanathan, S. and Vasudev, B., editors, *Visual Communications and Image Processing 2004*, volume 5308, pages 881 – 892. International Society for Optics and Photonics, SPIE.
- Chollet, F. (2017). Xception: Deep learning with depth-wise separable convolutions. *Proceedings - 30th IEEE Conference on Computer Vision and Pattern Recognition, CVPR 2017*, 2017-January:1800–1807.
- Christodoulidis, S. and Anthimopoulos, M. (2015). Food Recognition for Dietary Assessment Using Deep Convolutional Neural Networks Stergios. *New Trends in Image Analysis and Processing – ICIAP 2015 Workshops*, 9281(June):458–465.
- Cicuttin, A., Crespo, M. L., Mannatunga, K. S., Garcia, V. V., Baldazzi, G., Rignanese, L. P., Ahangarianabari, M., Bertuccio, G., Fabiani, S., Rachevski, A., Rashevskaya, I., Vacchi, A., Zampa, G., Zampa, N., Bellutti, P., Picciotto, A., Piemonte, C., and Zorzi, N. (2016). A programmable System-on-Chip based digital pulse processing for high resolution X-ray spectroscopy. *2016 International Conference on Advances in Electrical, Electronic and Systems Engineering, ICAEES 2016*, 15:520–525.
- Duchi, J. C., Bartlett, P. L., and Wainwright, M. J. (2012). Randomized smoothing for (parallel) stochastic optimization. *Proceedings of the IEEE Conference on Decision and Control*, 12:5442–5444.
- Flach, P., Hernández-Orallo, J., and Ferri, C. (2011). A coherent interpretation of AUC as a measure of aggregated classification performance. *Proceedings of the 28th International Conference on Machine Learning, ICML 2011*, (January 2014):657–664.
- Hafiz, A. M. and Bhat, G. M. (2020). A survey on instance segmentation: state of the art. *International Journal of Multimedia Information Retrieval*, 9(3):171–189.
- Ioffe, S. and Szegedy, C. (2015). Batch normalization: Accelerating deep network training by reducing internal covariate shift. *32nd International Conference on Machine Learning, ICML 2015*, 1:448–456.
- Kingma, D. P. and Ba, J. L. (2015). Adam: A method for stochastic optimization. *3rd International Conference on Learning Representations, ICLR 2015 - Conference Track Proceedings*, pages 1–15.
- Lim, L. A. and Keles, H. Y. (2019). Learning multi-scale features for foreground segmentation. *Pattern Analysis and Applications*, (0123456789).
- Lindgreen, A. and Lindgreen, A. (2004). Corruption and unethical behavior: report on a set of Danish guidelines. *Journal of Business Ethics*, 51(1):31–39.
- Liu, Y., Shen, C., Yu, C., and Wang, J. (2020). Efficient Semantic Video Segmentation with Per-frame Inference. pages 1–17.
- Minaee, S., Boykov, Y., Porikli, F., Plaza, A., Kehtarnavaz, N., and Terzopoulos, D. (2020). Image Segmentation Using Deep Learning: A Survey. pages 1–23.
- Parks, D. and Fels, S. (2008). Evaluation of background subtraction algorithms with post-processing. pages 192–199.
- Ramos, S., Rehfeld, T., Enzweiler, M., Benenson, R., and Roth, S. The Cityscapes Dataset for Semantic Urban Scene Understanding.
- Setitra, I. and Larabi, S. (2014). Background subtraction algorithms with post-processing: A review. *Proceedings - International Conference on Pattern Recognition*, pages 2436–2441.
- Simonyan, K. and Zisserman, A. (2015). Very deep convolutional networks for large-scale image recognition. *3rd International Conference on Learning Representations, ICLR 2015 - Conference Track Proceedings*, pages 1–14.
- Szegedy, C., Ioffe, S., Vanhoucke, V., and Alemi, A. A. (2017). Inception-v4, inception-ResNet and the impact of residual connections on learning. *31st AAAI Conference on Artificial Intelligence, AAAI 2017*, pages 4278–4284.
- Szegedy, C., Vanhoucke, V., Ioffe, S., Shlens, J., and Wojna, Z. (2016). Rethinking the Inception Architecture for Computer Vision. *Proceedings of the IEEE Computer Society Conference on Computer Vision and Pattern Recognition*, 2016-December:2818–2826.
- Wang, K., Gou, C., Zheng, N., Rehg, J. M., and Wang, F. Y. (2017a). Parallel vision for perception and understanding of complex scenes: methods, framework, and perspectives. *Artificial Intelligence Review*, 48(3):299–329.
- Wang, Y. (2014). Change detection 2014 challenge.
- Wang, Y., Jodoin, P. M., Porikli, F., Konrad, J., Benezech, Y., and Ishwar, P. (2014). CDnet 2014: An expanded change detection benchmark dataset. *IEEE Computer Society Conference on Computer Vision and Pattern Recognition Workshops*, pages 393–400.
- Wang, Y., Luo, Z., and Jodoin, P. M. (2017b). Interactive deep learning method for segmenting moving objects. *Pattern Recognition Letters*, 96:66–75.

- Yu, F. and Koltun, V. (2016). Multi-scale context aggregation by dilated convolutions. *4th International Conference on Learning Representations, ICLR 2016 - Conference Track Proceedings*.
- Zeiler, M. D. (2012). ADADELTA: An Adaptive Learning Rate Method.
- Zheng, W., Wang, K., and Wang, F. Y. (2020). A novel background subtraction algorithm based on parallel vision and Bayesian GANs. *Neurocomputing*, 394:178–200.